

Anomalous Hall Effect in Thick $\text{Co}_3\text{Sn}_2\text{S}_2$ Weyl Semimetal Crystals

Eddy Divin Kenvo Songwa,¹ Shaday Jesus Nobosse Nguemeta,¹ Hodaya Gabber,¹ Renana Aharonof,¹ and Dima Cheskis¹

Physics Department, Ariel University

(*Electronic mail: dimach@ariel.ac.il)

(Dated: 11 June 2025)

Ferromagnetic Weyl semimetals with Kagome lattice structures exhibit a strong coupling between magnetism and topological band features. $\text{Co}_3\text{Sn}_2\text{S}_2$ is a prime example, showing a giant anomalous Hall effect (AHE) driven by Berry curvature from the Weyl nodes. We investigated the temperature and angular dependence of Hall conductivity in thick $\text{Co}_3\text{Sn}_2\text{S}_2$ crystals, aiming to distinguish between topological and conventional magnetic contributions. Our measurements reveal an almost Hall response even at low magnetic fields and temperatures between 77 and 120 K, but are challenged by conventional magnetic contributions.

Ferromagnetic Weyl semimetals exhibit two closely interconnected phenomena. First, ferromagnetic materials exhibit magnetic ordering below the Curie temperature, resulting in itinerant magnetization and the breaking of time-reversal symmetry (TRS)¹. Second, in these materials, the combination of band crossings, spin-orbit coupling (SOC), and TRS breaking gives rise to topological effects, including the formation of topologically protected Weyl points^{2,3}. These Weyl points are sources or sinks of Berry curvature, often called “topological magnetic monopoles.”^{1,4}. A representative example is $\text{Co}_3\text{Sn}_2\text{S}_2$ ^{5–22}, in which both magnetic and topological features are realized within a Kagome lattice structure^{13,14,23,24}. A schematic representation is shown in Fig. 1.

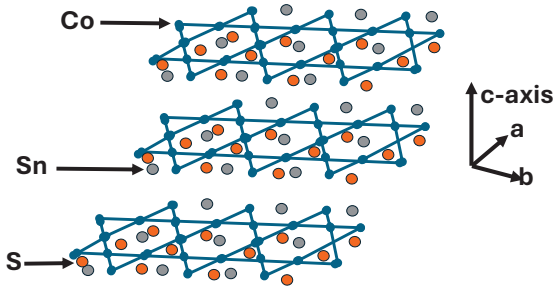


FIG. 1. Schematical model of $\text{Co}_3\text{Sn}_2\text{S}_2$.

Besides Co atoms, the nonmagnetic Sn and S atoms influence various aspects of magnetization. Co, Sn, and S form a layered Kagome structure that enhances domain wall pinning by introducing intrinsic anisotropy and potential trapping sites at the interlayer boundaries²⁵. Moreover, vacancies at Sn or S positions can act as structural defects, increasing coercivity by impeding domain wall motion²⁶. These nonmagnetic elements significantly alter the local coordination and symmetry around the Co sites, thereby modifying the spin-orbit interaction and influencing the magnetocrystalline anisotropy energy (MAE)^{19,27}. Although Sn and S atoms do not carry magnetic moments, their hybridization with Co 3d orbitals profoundly affects the electronic structure. This interaction alters the distribution of Berry curvature and governs the position

and separation of Weyl nodes. When the crystal is very thin, a quasi-two-dimensional model can somewhat approximate the described three-dimensional effects. However, such an approximation becomes invalid in materials with thicknesses of thousands of layers. In such cases, the system exhibits purely three-dimensional magnetic behavior.

Specifically, in $\text{Co}_3\text{Sn}_2\text{S}_2$, topological effects are confined to the c -axis, because the direction of the chiral topological vector^{8,28} is in the c -axis direction. To observe this effect, one must use angle-resolved photoemission spectroscopy (ARPES), which maps the electronic band structure $E(\mathbf{k})$ as a function of momentum. No other technique provides such direct visualization of band dispersion in momentum space^{29,30}. Observing open Fermi surfaces, or Fermi arcs, is a clear signature of Weyl semimetals¹⁰. However, ARPES cannot probe magnetic field dependence. Another key experimental method is the negative longitudinal magnetoresistance (NLMR) measurement, where resistance decreases under parallel electric and magnetic fields. This characteristic signature of Weyl fermions is linked to the chiral anomaly. Unlike classical magnetoresistance, it reflects charge pumping between Weyl nodes of opposite chirality. When combined with ARPES, which identifies Weyl cones and Fermi arcs, NLMR offers compelling evidence for Weyl semimetal behavior. The chiral magnetic effect—the generation of an electric current along a magnetic field due to a chiral chemical potential imbalance—is fundamental to this phenomenon^{31–34}. The main problem is that these measurements typically require high magnetic fields and low temperatures.

We aim to test the robustness of this effect under more practical conditions: temperatures above 77 K and low magnetic fields, by rotating the direction of the magnetic field.

It was shown that another phenomenon connected to Weyl topology is the AHE, which manifests as a transverse voltage in the absence of an external field. It has been demonstrated that in $\text{Co}_3\text{Sn}_2\text{S}_2$, the AHE is both large and stable over a range of temperatures, due to the stabilization of topological features by spin-orbit coupling^{35–38}. Furthermore, doping $\text{Co}_3\text{Sn}_2\text{S}_2$ with elements such as indium or nickel has enhanced the AHE^{39,40}.

Theoretically, the AHE can originate from intrinsic mechanisms (nonzero Berry curvature) or extrinsic mechanisms (side-jump or skew scattering)^{41,42}. In the inherent case, the

AHE is governed by the Berry curvature of the occupied bands, while the extrinsic contributions come from more classical reasons. It was previously shown that in $\text{Co}_3\text{Sn}_2\text{S}_2$, the easy axis of magnetization aligns along the c -axis, the direction of the chiral topological vector. To experimentally distinguish between classical and topological anomalous Hall conductivity.

The classical Hall voltage is^{43,44}:

$$V_{\text{Hall}} = \frac{IB}{nqt} = \frac{R_0IB}{t}, \quad (1)$$

with $R_0 = 1/(nq)$ the ordinary Hall coefficient. Including anomalous effects⁴¹:

$$-\rho_{xy} = R_0B + R_s\mu_0M, \quad (2)$$

, where R_0 and R_s are the ordinary and anomalous Hall coefficients, respectively. Usually, R_0 is much smaller than R_s , and the measurement at small external fields can be approximated to the anomalous Hall conductivity. The conductivity tensor yields:

$$\sigma_{xy}^A \approx \frac{R_s\mu_0M}{\rho_{xx}^2}. \quad (3)$$

While ρ_{xx} and R_s typically increase with temperature, M decreases, influencing the behavior of the AHE.

In topological Weyl systems, the anomalous Hall effect (AHE) originates from the Berry curvature and depends on temperature only through the Fermi–Dirac distribution, as shown in the following equation⁴⁵:

$$\sigma_{xy}^{\text{AHE}}(T) = -\frac{e^2}{\hbar} \sum_n \int_{\text{BZ}} \frac{d^3\mathbf{k}}{(2\pi)^3} f_n(\mathbf{k}, T) \Omega_n^z(\mathbf{k}), \quad (4)$$

where:

- $f_n(\mathbf{k}, T)$ is the Fermi–Dirac distribution function at temperature T ,
- $\Omega_n^z(\mathbf{k})$ is the z -component of the Berry curvature of band n at crystal momentum \mathbf{k} ,

and the integral is performed over the entire Brillouin zone (BZ).

As the temperature increases, the Fermi–Dirac distribution gradually smears around the Fermi energy. Because the Berry curvature sharply peaks near the Weyl nodes, which often lie close to the Fermi level, even small shifts in occupation near the Weyl nodes could significantly affect the integrated Berry curvature and hence AHC. As the temperature further increases and approaches the Curie point, the reduced magnetization diminishes the separation between Weyl nodes, thereby suppressing the topological contribution to the AHE¹⁰. We aim to identify a temperature regime in which the topological AHE remains robust against external magnetic field and temperature variations. To achieve this, we propose measuring the Hall effect in a thick ferromagnetic crystal as a function of magnetic field angle and temperature to differentiate between conventional and topological contributions.

In our experiment, we used a $670 \mu\text{m}$ -thick single crystal of $\text{Co}_3\text{Sn}_2\text{S}_2$. The crystallinity was confirmed using standard X-ray diffraction (XRD), and the elemental composition was verified by energy-dispersive X-ray spectroscopy (EDS) in a scanning electron microscope (SEM). Hall measurements were conducted using the LakeShore Cryotronics FastHall system, which employs an AC-based technique with a lock-in amplifier to enable fast measurements while minimizing noise and offset voltages. An external electromagnet was added to record the hysteresis loops characteristic of the ferromagnetic response. The system was initially cooled to 77 K using liquid nitrogen and then allowed to warm naturally to room temperature. Vacuum-insulated chamber walls helped maintain a slow temperature ramp, enabling complete hysteresis loop measurements at a nearly constant temperature.

The Hall response saturates as the field increases, consistent with ferromagnetic behavior. Angle-dependent coercivity indicates that the motion of the 3D domain influences the magnetization reversal. Fig. 2 shows different coercive fields for normal and angled orientations of the magnetic field to the surface plane of the material..

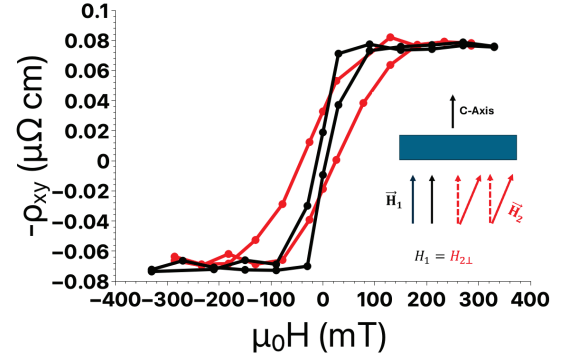


FIG. 2. Coercivity dependence for two field orientations.

Temperature-dependent Hall and longitudinal resistance measurements reveal three distinct temperature regions: (1) below 120 K, both ρ_{xx} and $-\rho_{xy}^A$ remain nearly constant; (2) between 120 K and 150 K, both quantities exhibit correlated variations; and (3) above 150 K, their behaviors diverge, suggesting a more complex interplay. This behavior is illustrated in Fig. 3.

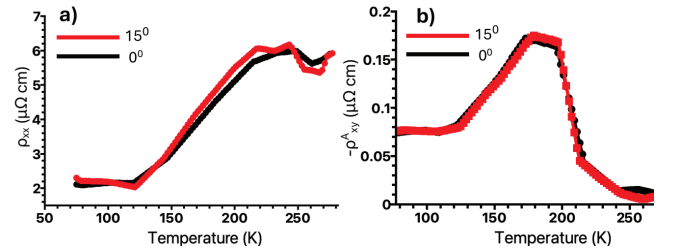


FIG. 3. Temperature dependence of (a) longitudinal resistivity ρ_{xx} and (b) anomalous Hall resistivity ρ_{xy} .

When comparing our results with those reported in the

literature³⁵, we observed that our measured ρ_{xy} is more than 200 times smaller, while ρ_{xx} is approximately 50 times smaller. Based on these values, we calculated the Hall conductivity σ_{xy} as a function of temperature for both 0° and 15° angles, as shown in Fig. 4.

Notably, the Hall conductivity in our measurements is more than 12 times larger than that reported by Liu et al.³⁵. This enhancement is primarily due to our sample's significantly lower longitudinal resistivity.

Furthermore, we found that the anomalous Hall conductivity (AHC) does not remain constant over any temperature range. However, up to 120 K, only minor variations are seen at both angles, with a near match around 105 K. Between 120 K and 145 K, σ_{xy} gradually decreases, again showing agreement at around 135 K. Above 145 K, noticeable differences between the two measurement angles begin to appear.

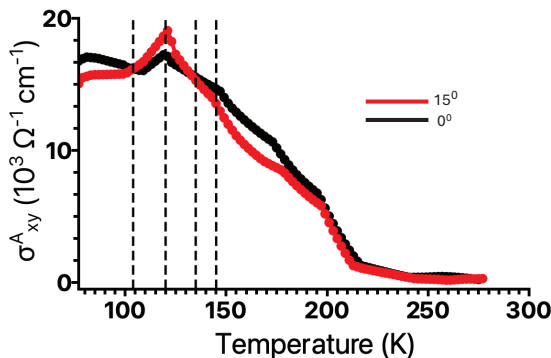


FIG. 4. Hall conductivity, σ_{xy}^A , as a function of temperature.

Analyzing our results, we find that despite measuring a very thick sample, the behavior of the Hall conductivity is consistent with what is reported in the literature. Moreover, the measured Hall conductivity is even larger than previously reported values. This enhancement is attributed to the significantly higher longitudinal conductivity, likely due to the greater thickness of the conducting material.

Examining the σ_{xy}^A graph, we suggest that topological effects may dominate up to 120 K, although their exact contribution remains uncertain. Even within the 77–120 K range, small fluctuations in Hall conductivity are observed, which depend on the magnetization orientation. Between 120 K and 145 K, the Hall conductivity decreases steadily with nearly the same slope for both magnetization angles, indicating that the topological Weyl contribution may still be present.

Above 145 K, σ_{xy}^A behavior appears to be primarily governed by conventional magnetic effects, as the conductivity decreases similarly for both angles. However, the anomalous Hall effect (AHE) becomes strongly angle-dependent beyond this point, suggesting increased complexity in the underlying mechanisms.

Overall, our measurements show that even in the low-temperature range (77–120 K), isolating a purely topological contribution to the AHE is difficult. The results indicate a complex interplay between topological and magnetic effects across all temperature regions, making it challenging to at-

tribute the Hall conductivity to a single origin. Further investigation is planned to resolve better the magnetic contributions, particularly in the high-temperature regime where the AHC behavior begins to diverge significantly.

Our study demonstrates that the topological contribution to the anomalous Hall effect (AHE) in $\text{Co}_3\text{Sn}_2\text{S}_2$ remains substantial up to approximately 120 K. In the intermediate temperature range of 120–145 K, the observed decrease in anomalous Hall conductivity (AHC) is likely driven by reduced magnetization and thermal broadening of the Fermi–Dirac distribution near the Fermi level. Such an explanation is supported by the similar behavior of AHC at both measurement angles.

Above 145 K, magnetic behavior becomes more complex, suggesting the involvement of additional mechanisms. Due to the considerable thickness of the crystal, small temperature gradients may persist within the sample, possibly explaining the residual Hall conductivity observed even at 175 K.

ACKNOWLEDGMENTS

The authors thank Professor Yuri Gorodetski for insightful discussions.

- ¹N. P. Armitage, E. J. Mele, and A. Vishwanath, *Reviews of Modern Physics* **90**, 015001 (2018), arXiv:1705.01111.
- ²B. Yan and C. Felser, *Annual Review of Condensed Matter Physics* **8**, 337 (2017).
- ³A. A. Burkov, *Annual Review of Condensed Matter Physics* **9**, 359 (2018).
- ⁴S. Y. Xu, I. Belopolski, N. Alidoust, M. Neupane, G. Bian, C. Zhang, R. Sankar, G. Chang, Z. Yuan, C. C. Lee, S. M. Huang, H. Zheng, J. Ma, D. S. Sanchez, B. K. Wang, A. Bansil, F. Chou, P. P. Shibayev, H. Lin, S. Jia, and M. Z. Hasan, *Science* **349**, 613 (2015), arXiv:1502.03807.
- ⁵B. He, T. Yu, Y. Pan, C. Le, D. Chen, Y. Sun, and C. Felser, *Physical Review B* **111**, 45157 (2025).
- ⁶M. Kanagaraj, J. Ning, and L. He, *Reviews in Physics* **8**, 100072 (2022).
- ⁷D. F. Liu, Q. N. Xu, E. K. Liu, J. L. Shen, C. C. Le, Y. W. Li, D. Pei, A. J. Liang, P. Dudin, T. K. Kim, C. Cacho, Y. F. Xu, Y. Sun, L. X. Yang, Z. K. Liu, C. Felser, S. S. P. Parkin, and Y. L. Chen, *Physical Review B* **104**, 205140 (2021).
- ⁸L. Ye, M. Kang, J. Liu, F. Von Cube, C. R. Wicker, T. Suzuki, C. Jozwiak, A. Bostwick, E. Rotenberg, and D. C. Bell, *Nature* **555**, 638 (2018).
- ⁹S. E. Pate, B. Wang, Y. Zhang, B. Shen, E. Liu, I. Martin, J. S. Jiang, X. Zhou, D. Y. Chung, and M. G. Kanatzidis, *Advanced Science* **11**, 2406882 (2024).
- ¹⁰A. Rossi, V. Ivanov, S. Sreedhar, A. L. Gross, Z. Shen, E. Rotenberg, A. Bostwick, C. Jozwiak, V. Taufour, S. Y. Savrasov, and I. M. Vishik, *Physical Review B* **104**, 155115 (2021).
- ¹¹I. Belopolski, T. A. Cochran, X. Liu, Z.-J. Cheng, X. P. Yang, Z. Guguchia, S. S. Tsirkin, J.-X. Yin, P. Vir, G. S. Thakur, S. S. Zhang, J. Zhang, K. Kaznatcheev, G. Cheng, G. Chang, D. Multer, N. Shumiya, M. Litskevich, E. Vescovo, T. K. Kim, C. Cacho, N. Yao, C. Felser, T. Neupert, and M. Z. Hasan, *Physical Review Letters* **127**, 256403 (2021).
- ¹²J. Liu, Y. Yang, J. Shen, D. Liu, G. S. Thakur, C. Guillemard, A. Smekhova, H. Chen, D. Biswas, M. Valvidares, E. Liu, C. Felser, T.-L. Lee, T. Hesjedal, Y. Chen, and G. van der Laan, *ACS Nano* **19**, 8561 (2025).
- ¹³D. Chen, C. Le, C. Fu, H. Lin, W. Schnelle, Y. Sun, and C. Felser, *Physical Review B* **103**, 144410 (2021).
- ¹⁴B. Lv, R. Zhong, X. Luo, S. Ma, C. Chen, S. Wang, Q. Luo, F. Gao, C. Fang, and W. Ren, *Scripta Materialia* **255**, 116345 (2025).
- ¹⁵L. Wang, G. Tian, H. Chen, J. Zhao, H. Shi, H. Wang, Z. Li, and X. Wu, *Physical Review B* **111**, 54412 (2025).
- ¹⁶J. Ikeda, K. Fujiwara, J. Shiogai, T. Seki, K. Nomura, K. Takanashi, and A. Tsukazaki, *Communications Materials* **2**, 18 (2021).
- ¹⁷I. V. Solovyev, S. A. Nikolaev, A. V. Ushakov, V. Y. Irkhin, A. Tanaka, and S. V. Streltsov, *Physical Review B* **105**, 14415 (2022).

- ¹⁸S. E. Pate, B. Wang, B. Shen, J. S. Jiang, U. Welp, W.-K. Kwok, J. Xu, K. Li, R. Divan, and Z.-L. Xiao, *Physical Review B* **108**, L100408 (2023).
- ¹⁹J. Shen, Q. Zeng, S. Zhang, W. Tong, L. Ling, C. Xi, Z. Wang, E. Liu, W. Wang, G. Wu, and B. Shen, *Applied Physics Letters* **115**, 212403 (2019).
- ²⁰I. Živković, R. Yadav, J.-R. Soh, C. Yi, Y. Shi, O. V. Yazyev, and H. M. Rønnow, *Physical Review B* **106**, L180403 (2022).
- ²¹W. Yan, X. Zhang, Q. Shi, X. Yu, Z. Zhang, Q. Wang, S. Li, and H. Lei, *Solid State Communications* **281**, 57 (2018).
- ²²N. N. Orlova, V. D. Esin, A. V. Timonina, N. N. Kolesnikov, and E. V. Deviatov, *Journal of Magnetism and Magnetic Materials* **624**, 172998 (2025).
- ²³Q. Wang, H. Lei, Y. Qi, and C. Felser, *Accounts of Materials Research* **5**, 786 (2024).
- ²⁴Q. Zhang, Y. Zhang, M. Matsuda, V. O. Garlea, J. Yan, M. A. McGuire, D. A. Tennant, and S. Okamoto, *Journal of the American Chemical Society* **144**, 14339 (2022).
- ²⁵C. Lee, P. Vir, K. Manna, C. Shekhar, J. E. Moore, M. A. Kastner, C. Felser, and J. Orenstein, *Nature Communications* **13**, 3000 (2022).
- ²⁶J. Shiogai, J. Ikeda, K. Fujiwara, T. Seki, K. Takahashi, and A. Tsukazaki, *Physical Review Materials* **6**, 114203 (2022).
- ²⁷J. Shiogai, J. Ikeda, K. Fujiwara, T. Seki, K. Takahashi, and A. Tsukazaki, *Physical Review Materials* **5**, 24403 (2021).
- ²⁸S. Nakatsuji, N. Kiyohara, and T. Higo, *Nature* **527**, 212 (2015).
- ²⁹D. F. Liu, E. K. Liu, Q. N. Xu, J. L. Shen, Y. W. Li, D. Pei, A. J. Liang, P. Dudin, T. K. Kim, C. Cacho, Y. F. Xu, Y. Sun, L. X. Yang, Z. K. Liu, C. Felser, S. S. P. Parkin, and Y. L. Chen, *npj Quantum Materials* **7**, 11 (2022).
- ³⁰H. Lohani, P. Foulquier, P. Le Fèvre, F. Bertran, D. Colson, A. Forget, and V. Broutet, *Physical Review B* **107**, 245119 (2023).
- ³¹S. Kaushik, D. E. Kharzeev, and E. J. Philip, *Physical Review B* **99**, 75150 (2019).
- ³²D. E. Kharzeev and H.-U. Yee, *Physical Review B* **88**, 115119 (2013).
- ³³A. Cortijo, D. Kharzeev, K. Landsteiner, and M. A. H. Vozmediano, *Physical Review B* **94**, 241405 (2016).
- ³⁴D. E. Kharzeev, Y. Kikuchi, R. Meyer, and Y. Tanizaki, *Physical Review B* **98**, 14305 (2018).
- ³⁵E. Liu, Y. Sun, N. Kumar, L. Muechler, A. Sun, L. Jiao, S.-Y. Yang, D. Liu, A. Liang, Q. Xu, J. Kroder, V. Süß, H. Borrmann, C. Shekhar, Z. Wang, C. Xi, W. Wang, W. Schnelle, S. Wirth, Y. Chen, S. T. B. Goennenwein, and C. Felser, *Nature Physics* **14**, 1125 (2018).
- ³⁶Q. Wang, Y. Xu, R. Lou, Z. Liu, M. Li, Y. Huang, D. Shen, H. Weng, S. Wang, and H. Lei, *Nature Communications* **9**, 3681 (2018).
- ³⁷S.-Y. Yang, J. Noky, J. Gayles, F. K. Dejene, Y. Sun, M. Dörr, Y. Skourski, C. Felser, M. N. Ali, E. Liu, and S. S. P. Parkin, *Nano Letters* **20**, 7860 (2020).
- ³⁸Y.-C. Lau, J. Ikeda, K. Fujiwara, A. Ozawa, J. Zheng, T. Seki, K. Nomura, L. Du, Q. Wu, A. Tsukazaki, and K. Takahashi, *Physical Review B* **108**, 64429 (2023).
- ³⁹G. S. Thakur, P. Vir, S. N. Guin, C. Shekhar, R. Wehrich, Y. Sun, N. Kumar, and C. Felser, *Chemistry of Materials* **32**, 1612 (2020).
- ⁴⁰H. Zhou, G. Chang, G. Wang, X. Gui, X. Xu, J.-X. Yin, Z. Guguchia, S. S. Zhang, T.-R. Chang, H. Lin, W. Xie, M. Z. Hasan, and S. Jia, *Physical Review B* **101**, 125121 (2020).
- ⁴¹N. Nagaosa, J. Sinova, S. Onoda, A. H. MacDonald, and N. P. Ong, *Reviews of Modern Physics* **82**, 1539 (2010).
- ⁴²A. Burkov, *Physical Review Letters* **113**, 187202 (2014).
- ⁴³N. W. Ashcroft and N. D. Mermin, *Solid State Physics* (Brooks/Cole, Belmont, California, 1976).
- ⁴⁴J. M. Ziman, *Principles of the Theory of Solids*, 2nd ed. (Cambridge University Press, Cambridge, 1972).
- ⁴⁵D. Xiao, M.-C. Chang, and Q. Niu, *Reviews of Modern Physics* **82**, 1959 (2010).